Static thermo-optic instability in double-pass fiber amplifiers

Lægsgaard, Jesper

Published in:
Optics Express

Link to article, DOI:
10.1364/OE.24.013429

Publication date:
2016

Document Version
Publisher's PDF, also known as Version of record

Static thermo-optic instability in double-pass fiber amplifiers

Jesper Lægsgaard

DTU Fotonik, Department of Photonics Engineering, Technical University of Denmark, Ørsteds Plads 343, DK-2800 Kongens Lyngby, Denmark

jlag@fotonik.dtu.dk

Abstract: A coupled-mode formalism, earlier used to describe transverse mode instabilities in single-pass optical fiber amplifiers, is extended to the case of double-pass amplifiers. Contrary to the single-pass case, it is shown that the thermo-optic nonlinearity can couple light at the same frequency between the LP_{01} and LP_{11} modes, leading to a static deformation of the output beam profile. This novel phenomenon is caused by the interaction of light propagating in either direction with thermo-optic index perturbations caused by light propagating in the opposite direction. The threshold power for the static deformation is found to be several times lower than what is typically found for the dynamic modal instabilities observed in single-pass amplifiers.

OCIS codes: (140.3510) Lasers, fiber; (140.6810) Thermal effects; (060.2320) Fiber optics amplifiers and oscillators.

References and links

1. T. Eidam, C. Wirth, C. Jauregui, F. Stutzki, F. Jansen, H.-J. Otto, O. Schmidt, T. Schreiber, J. Limpert, and A. Tünnermann, "Experimental observations of the threshold-like onset of mode instabilities in high power fiber amplifiers," Opt. Express **19**, 13218–13224 (2011).
2. A. V. Smith and J. J. Smith, "Mode instability in high power fiber amplifiers," Opt. Express **19**, 10180–10192 (2011).
3. K. R. Hansen, T. T. Alkeskjold, J. Broeng, and J. Lægsgaard, "Thermally induced mode coupling in rare-earth doped fiber amplifiers," Opt. Lett. **37**, 2382–2384 (2012).
4. B. G. Ward, "Modeling of transient modal instability in fiber amplifiers," Opt. Express **21**, 12053–12067 (2013).
5. L. Dong, "Stimulated thermal rayleigh scattering in optical fibers," Opt. Express **21**, 2642–2656 (2013).
6. K. R. Hansen, T. T. Alkeskjold, J. Broeng, and J. Lægsgaard, "Theoretical analysis of mode instability in high-power fiber amplifiers," Opt. Express **21**, 1944–1971 (2013).
7. C. Jauregui, H.-J. Otto, F. Stutzki, J. Limpert, and A. Tünnermann, "Simplified modelling the mode instability threshold of high power fiber amplifiers in the presence of photodarkening," Opt. Express **23**, 20203–20218 (2015).
8. A. Galvanauskas, G. Cho, A. Hariharan, M. Fermann, and D. Harter, "Generation of high-energy femtosecond pulses in multimode-core Yb-fiber chirped-pulse amplification systems," Opt. Lett. **26**, 935–937 (2001).
9. J. R. Marciante and J. D. Zuegel, "High-gain, polarization-preserving, Yb-doped fiber amplifier for low-duty-cycle pulse amplification," Appl. Optics **45**, 6798–6804 (2006).
10. P.-Y. Lai, C.-L. Chang, S.-L. Huang, and S.-H. Chen, "Effective suppression of stimulated Raman scattering in high power fiber amplifiers using double-pass scheme," in "FIBER LASERS XI: TECHNOLOGY, SYSTEMS, AND APPLICATIONS," , vol. 8961 of *Proceedings of SPIE*, Ramachandran, S, ed., SPIE; NKT Photon A S; PolarOnyx, Inc (SPIE-INT SOC OPTICAL ENGINEERING, 1000 20TH ST, PO BOX 10, BELLINGHAM, WA 98227-0010 USA, 2014), vol. 8961 of *Proceedings of SPIE*. Conference on Fiber Lasers XI - Technology, Systems, and Applications, San Francisco, CA, FEB 03-06, 2014.
11. K. R. Hansen and J. Lægsgaard, "Impact of gain saturation on the mode instability threshold in high-power fiber amplifiers," Opt. Express **22**, 11267–11278 (2014).

#262186 Received 30 Mar 2016; revised 27 May 2016; accepted 6 Jun 2016; published 9 Jun 2016

12. M. Yamada and K. Sakuda, "Analysis of almost-periodic distributed feedback slab waveguides via a fundamental matrix approach," Appl. Opt. **26**, 3474–3478 (1987).
13. W. H. Press, B. P. Flannery, S. A. Teukolsky, and W. T. Vetterling, *Numerical Recipes in Fortran 77* (Cambridge University, 2001).
14. A. V. Smith and J. J. Smith, "Increasing mode instability thresholds of fiber amplifiers by gain saturation," Opt. Express **21**, 15168–15182 (2013).
15. J. Lægsgaard, "Optimizing Yb concentration of fiber amplifiers in the presence of transverse modal instabilities and photodarkening," Appl. Opt. **55**, 1966–1970 (2016).
16. C. Jauregui, H. J. Otto, J. Limpert, and A. Tünnermann, "Mode instabilities in high-power bidirectional fiber amplifiers and lasers," in "Advanced Solid State Lasers," (Optical Society of America, 2015), p. ATh2A.24.
17. O. Antipov, M. Kuznetsov, V. Tyrtyshnyy, D. Alekseev, and O. Vershinin, "Low-threshold mode instability in yb3+-doped few-mode fiber amplifiers: influence of a backward reflection," Proc. SPIE **9728**, 97280A (2016).
18. K. Hejaz, A. Norouzey, R. Poozesh, A. Heidariazar, A. Roohforouz, R. R. Nasirabad, N. T. Jafari, A. H. Golshan, A. Babazadeh, and M. Lafouti, "Controlling mode instability in a 500 W ytterbium-doped fiber laser," Laser Physics **24**, 025102 (2014).

1. Introduction

Transverse modal instabilities (TMI) presently constitute the main limiting factor for average-power scaling of Yb-doped fiber amplifier systems with large cores [1, 2]. It is by now broadly recognized that the main cause of TMI is thermo-optic nonlinear coupling between the fundamental mode (FM) and first higher-order mode (HOM) of the fiber [2–7]. One may picture this coupling as being due to a self-written long-period grating arising from the longitudinally periodic variation in heat load caused by beating between the FM and HOM, which by definition has the periodicity needed for coupling light between the two modes. It can be shown, however, that efficient coupling can only occur if the HOM is slightly downshifted in frequency with respect to the FM, so that a moving grating is created [2, 3]. This is in analogy with the well-known Raman effect in nonlinear optics, where a delayed nonlinear response leads to a downshift in frequency of the propagating light, and indeed the same kind of exponential amplification is found in numerical simulations [3,6]. In the case of thermo-optic nonlinearities, the downshift is on the kHz or sub-kHz level, due to the long thermal response times, and the upshot of the process is therefore an output beam profile which oscillates at this timescale. The seed for the low-frequency HOM signal may be quantum noise, or amplitude noise in the small fraction of seed signal (typically a few percent) accidentially coupled into the HOM [6]. It follows that TMI in single-pass amplifiers is inherently a dynamic phenomenon.

Since high-power fiber laser systems typically contain a series of amplifier stages, with large-mode area (LMA) fibers being incorporated in the high-power part of the chain, it is of interest to implement double-pass amplifiers at power levels exceeding 100 W. This would allow to simplify the system by using fewer amplifier fibers, and associated components for pump coupling, cooling etc., and an advanced LMA fiber (*e.g.* a photonic crystal rod fiber, or the like) may in effect be utilized for two amplification stages. The usefulness of double-pass amplification schemes for short-pulsed fiber laser systems has been demonstrated by several authors [8–10]. So far, however, no results have been published in the power regime where TMI becomes problematic for single-pass amplifiers (typically 2-300 W, with some dependence on system and fiber design). From a theoretical perspective, the case of a double-pass amplifier is different from the single-pass case because both forward- and backward-propagating signals can generate thermo-optic index gratings, and the grating created by signals propagating in either direction can scatter the light propagating in the opposite direction as well. Therefore, one cannot expect that thermo-optic nonlinear effects in double-pass amplifiers will be a simple generalization of the phenomena observed in the single-pass case.

In this paper, thermo-optic couplings between the FM and HOM of a two-mode fiber amplifier in a double-pass configuration are analyzed numerically. An established coupled-

#262186 Received 30 Mar 2016; revised 27 May 2016; accepted 6 Jun 2016; published 9 Jun 2016

mode model for single-pass amplifiers [3, 11] is generalized to the double-pass case by considering a refractive-index perturbation arising from signals propagating in both directions. It is predicted that, contrary to the single-pass case, the double-pass amplifier may suffer from a *static* thermo-optic instability phenomenon, whose origin and properties are qualitatively different from single-pass TMI. Whereas the phase relationship between two co-propagating modes and the grating they create forbids efficient power transfer between modes at the same frequency, this is not so for a grating arising from modes propagating in the opposite direction. The instability may set in at power levels below 50 W, several times lower than the typical threshold for dynamic TMI. In the strongly coupled regime, multiple solutions of the coupled-mode equations for the modal powers along the amplifier are found for a given pump power level. One could therefore expect to observe a quasi-static behaviour, with the mode profile jumping between different stability points, in a practical realization.

The paper is organized as follows: In section 2, the numerical model for calculating the effects of a static thermo-optic nonlinearity is laid out, and the numerical approach to solving the resulting coupled nonlinear equations is discussed. In section 3, numerical results are presented and analyzed for a particular double-pass amplifier, and some design modifications are considered. Section 4 discusses existing experimental results in connection with the new theory presented, whereas section 5 summarizes the conclusions.

2. Formal theory

The system to be considered is a cladding-pumped fiber amplifier of length L, with pump and seed signal launched at the same end, in the 'forward' direction. The signal light is reflected at the far end of the amplifier, to traverse the fiber once more in the 'backward' direction, with output signal thus being collected in the same end as input signal is launched. In practical systems, this is realized by a polarization rotation upon reflection, and the use of a polarization beam splitter at the input/output end.

The total electric field of forward and backward propagating radiation is written as

$$E_+(\mathbf{r},t) = \frac{1}{\sqrt{2}}\left[a_{1+}(z)e^{i(\omega t-\beta_1 z)}\Psi_1(\mathbf{r}_\perp) + a_{2+}(z)e^{i(\omega t-\beta_2 z)}\Psi_2(\mathbf{r}_\perp) + c.c.\right] \quad (1)$$

$$E_-(\mathbf{r},t) = \frac{1}{\sqrt{2}}\left[a_{1-}(z)e^{i(\omega t+\beta_1 z)}\Psi_1(\mathbf{r}_\perp) + a_{2-}(z)e^{i(\omega t+\beta_2 z)}\Psi_2(\mathbf{r}_\perp) + c.c.\right] \quad (2)$$

with +/- indices denoting forward and backward propagating fields respectively. Here ω is the signal frequency, β_1, β_2 are the propagation constants of the two modes considered in the expansion, and *c.c.* denotes a complex conjugate. The total average intensity of the field is given by

$$\begin{aligned} I(\mathbf{r}) = I_+(\mathbf{r}) + I_-(\mathbf{r}) = &\mid a_{1+}(z)\mid^2 \mid \Psi_1(\mathbf{r}_\perp)\mid^2 + \mid a_{2+}(z)\mid^2 \mid \Psi_2(\mathbf{r}_\perp)\mid^2 + \\ &2\mathrm{Re}\left[a_{1+}^*(z)a_{2+}(z)e^{i\Delta\beta z}\Psi_1^*(\mathbf{r}_\perp)\Psi_2(\mathbf{r}_\perp)\right] + \mid a_{1-}(z)\mid^2 \mid \Psi_1(\mathbf{r}_\perp)\mid^2 + \\ &\mid a_{2-}(z)\mid^2 \mid \Psi_2(\mathbf{r}_\perp)\mid^2 + 2\mathrm{Re}\left[a_{1-}^*(z)a_{2-}(z)e^{-i\Delta\beta z}\Psi_1^*(\mathbf{r}_\perp)\Psi_2(\mathbf{r}_\perp)\right] \end{aligned} \quad (3)$$

with $\Delta\beta$=$\beta_1 - \beta_2$. Interference terms between forward- and backward-propagating fields have been omitted for two reasons: Firstly, as mentioned above, a double-pass configuration is typically realized by a polarization rotation, and orthogonal polarizations do not interfere. Secondly, if amplification of pulses much shorter than the length of the amplifier (*e.g.* picosecond or few-nanosecond pulses) is considered, forward- and backward-propagating light will not be simultaneously present in the fiber. Thus, the present approach may also be justified

#262186 Received 30 Mar 2016; revised 27 May 2016; accepted 6 Jun 2016; published 9 Jun 2016

in for short pulses in laser cavities without polarization rotation upon reflection. On the other hand, to model a continuous-wave (CW) laser cavity, or end facet reflection from a single-pass amplifier, additional interference terms may need to be taken into account.

The heat load at a given point in the doped core is given by the local intensity and gain as

$$Q(\mathbf{r}) = \left(\frac{\omega_p}{\omega} - 1\right) I(\mathbf{r}) g(\mathbf{r}) = I(\mathbf{r}) \frac{g_0(z)}{1 + \frac{I(\mathbf{r})}{I_{sat}(z)}} \tag{4}$$

where ω_p is the pump frequency, and the local gain parameters $g_0(z)$, $I_{sat}(z)$ are given by

$$g_0(z) = N_{Yb} \frac{I_p(z)(\sigma_{ap}\sigma_{es} - \sigma_{as}\sigma_{ep}) - P_\tau \sigma_{as}}{I_p(z)(\sigma_{ap} + \sigma_{ep}) + P_\tau} \tag{5}$$

$$I_{sat}(z) = \frac{\omega}{\omega_p} \frac{I_p(z)(\sigma_{ap} + \sigma_{ep}) + P_\tau}{\sigma_{as} + \sigma_{es}} \tag{6}$$

$$P_\tau = \frac{\hbar \omega_p}{\tau};\ I_p(z) = \frac{P_p(z)}{A_p} \tag{7}$$

Here A_p is the area of the inner cladding, and it is assumed that the pump power, $P_p(z)$ is evenly distributed over this area. τ is the relaxation time of the Yb upper-state level, and $\sigma_{ap}, \sigma_{ep}, \sigma_{as}, \sigma_{es}$ are the absorption/emission cross sections of pump and signal respectively.

The heat load leads to a real-valued index perturbation in the fiber through the thermo-optic effect. In addition, the gain can be described as an imaginary contribution to the refractive index, or equivalently, the relative permittivity. The total permittivity perturbation from gain and thermo-optic effects can be written as:

$$\Delta\varepsilon(\mathbf{r}) = \frac{\eta}{\kappa} \int d\mathbf{r}'_\perp G(\mathbf{r}_\perp, \mathbf{r}'_\perp) Q(\mathbf{r}'_\perp, z) + i \frac{g_0(z)}{1 + \frac{I(\mathbf{r})}{I_{sat}(z)}} \frac{n_0}{k_0} \tag{8}$$

with n_0 being the refractive index of the fiber, and k_0 the vacuum wave number of the signal. η is the thermo-optic coefficient of the glass, and κ is its thermal conductivity. Assuming a cylindrical fiber with homogeneous thermal properties, the Green's function G can be written in a cylindrical coordinate expansion as

$$G(\mathbf{r}_\perp, \mathbf{r}'_\perp) = \frac{1}{2\pi} \sum_{m=-\infty}^{\infty} G_m(r, r') e^{im(\phi - \phi')} \tag{9}$$

The G_m functions are evaluated using the expressions given by Hansen *et al* [3] in the static (zero-frequency) limit.

The evolution of forward- and backward-propagating signals in the two modes can be described in coupled-mode theory as

$$\frac{da_{1+}}{dz} = -i \frac{k_0}{2n_0} \left[a_{1+}(z)\Delta\varepsilon_{11}(z) + a_{2+}(z) e^{i\Delta\beta z} \Delta\varepsilon_{12}(z) \right] \tag{10}$$

$$\frac{da_{2+}}{dz} = -i \frac{k_0}{2n_0} \left[a_{2+}(z)\Delta\varepsilon_{22}(z) + a_{1+}(z) e^{-i\Delta\beta z} \Delta\varepsilon_{12}(z) \right] \tag{11}$$

$$\frac{da_{1-}}{dz} = i \frac{k_0}{2n_0} \left[a_{1-}(z)\Delta\varepsilon_{11}(z) + a_{2-}(z) e^{-i\Delta\beta z} \Delta\varepsilon_{12}(z) \right] \tag{12}$$

$$\frac{da_{2-}}{dz} = i \frac{k_0}{2n_0} \left[a_{2-}(z)\Delta\varepsilon_{22}(z) + a_{1-}(z) e^{i\Delta\beta z} \Delta\varepsilon_{12}(z) \right] \tag{13}$$

#262186 Received 30 Mar 2016; revised 27 May 2016; accepted 6 Jun 2016; published 9 Jun 2016

with $\Delta\varepsilon_{mn}$ being given by

$$\Delta\varepsilon_{mn}(z) = \int d\mathbf{r}_\perp \Psi_m^*(\mathbf{r}_\perp)\Delta\varepsilon(\mathbf{r})\Psi_n(\mathbf{r}_\perp) \tag{14}$$

The first terms on the right-hand side of these equations include amplifier gain as well as self- and cross-phase modulation effects arising from the thermo-optic nonlinearity. The second terms describe scattering between co-propagating FM and HOM modes due to thermo-optic effects ('thermal gratings'). In addition, if the pump power is evenly distributed over the inner cladding, as is commonly assumed, it will obey the evolution equation

$$\frac{dP_p}{dz} = -P_p\frac{N_{Yb}}{A_p}\int_{A_d} d\mathbf{r}_\perp\left[\sigma_{ap} - n_2(\mathbf{r}_\perp,z)(\sigma_{ap}+\sigma_{ep})\right] \tag{15}$$

with $n_2(\mathbf{r}_\perp,z)$ given by

$$n_2(\mathbf{r}_\perp,z) = \frac{g_0(z)}{N_{Yb}(\sigma_{as}+\sigma_{es})\left(1+\frac{I_s(r,z)}{I_{sat}(z)}\right)} + \frac{\sigma_{as}}{\sigma_{as}+\sigma_{es}} \tag{16}$$

The term $\left(1+\frac{I_s(r,z)}{I_{sat}(z)}\right)$ in the denominator expresses the effect of gain saturation. Here it has been utilized that the pumping is in the forward direction, which is advantageous with respect to mitigation of Kerr and Raman nonlinearities because it gives the strongest amplification close to the final output, corresponding to backward pumping in a single-pass amplifier.

These equations should be solved subject to appropriate boundary conditions for the reflection of FM and HOM signals at the far end of the amplifier:

$$a_{m-}(L) = a_{m+}(L)R_m;\ \ R_m = r_m e^{i\phi_m}e^{-2i\beta_m L},\ \ m = 1,2 \tag{17}$$

where r_m represents the magnitude of reflection for mode m, ϕ_m represents a phase change upon reflection, and the factor $e^{-2i\beta_m L}$ ensures that r_m=1, ϕ_m=0 corresponds to a direct reflection at the end facet. With this formulation, Eqs. (10)-(13) and (15) can be regarded as four nonlinear equations in four real variables, namely the real and imaginary parts of the final output fields $a_{1-}(0)$ and $a_{2-}(0)$. These values should be determined so that propagation of Eqs. (10)-(13) and (15) from z=0 to z=L lead to final amplitudes satisfying Eq. (17). This is in general a non-trivial task, as will be discussed in the next section.

For a single-pass amplifier, the FM and HOM output amplitudes are uniquely determined by the input amplitudes, through the propagation equations (10) and (11), when stripped of their contributions from backward-propagating modes. Similarly, if all $a_{m\pm}(0)$ amplitudes were specified for the double-pass amplifier, the $a_{m\pm}(0)$ would be uniquely determined by propagating Eqs. (10)-(13). However, the $a_{m-}(0)$ amplitudes are not known *a priori*. Instead, one has the boundary conditions in Eq. (17). The resulting system of nonlinear equations is not guaranteed to have unique solutions for a given value of the $a_{m+}(0)$ input coefficients.

A considerable simplification of Eqs. (10)-(13) may be obtained if one adopts the undepleted-pump approximation, *i.e.* the assumption that $a_{2\pm}(z) << a_{1\pm}(z)$ everywhere, so that depletion of the latter may be neglected. In this case, the $a_{2\pm}$ terms may be dropped from Eqs. (10) and (12), which may then be solved for a rotationally invariant power distribution. In the present work, the transverse field distributions are taken to be

$$\Psi_1(\mathbf{r}_\perp) = \frac{1}{\sqrt{2\pi}}R_1(r);\ \ \Psi_2(\mathbf{r}_\perp) = \frac{1}{\sqrt{\pi}}R_2(r)\frac{x}{r} \tag{18}$$

#262186 Received 30 Mar 2016; revised 27 May 2016; accepted 6 Jun 2016; published 9 Jun 2016

with R_1, R_2 being the radial mode profiles of LP_{01} and LP_{11} modes respectively. The resulting equations can be written as

$$\frac{da_{1+}}{dz} = \left[g_{11}(z) - \frac{i}{2}\left(\mid a_{1+}(z) \mid^2 + \mid a_{1-}(z) \mid^2 \right) G_{11}(z) \right] a_{1+}(z) \tag{19}$$

$$\frac{da_{1-}}{dz} = -\left[g_{11}(z) - \frac{i}{2}\left(\mid a_{1+}(z) \mid^2 + \mid a_{1-}(z) \mid^2 \right) G_{11}(z) \right] a_{1-}(z) \tag{20}$$

$$g_{11}(z) = g_0(z) \int_0^{r_d} dr\, r \frac{R_1^2(r)}{1 + \frac{I_0(r,z)}{I_{sat}(z)}} \tag{21}$$

$$I_0(r,z) = \left(\mid a_{1+}(z) \mid^2 + \mid a_{1-}(z) \mid^2 \right) \frac{R_1^2(r)}{2\pi} \tag{22}$$

$$G_{11}(z) = \frac{\eta k_0 \left(\frac{\omega_p}{\omega} - 1 \right)}{2\pi n_0 \kappa} g_0(z) \int dr\, r R_1^2(r) \int dr' r' G_0(r,r') \frac{R_1^2(r')}{1 + \frac{I_0(r',z)}{I_{sat}(z)}} \tag{23}$$

The g_{11}-terms express amplifier gain, whereas the G_{11} terms describe self- and cross-phase modulation from the thermo-optic nonlinearity. Having established $a_{1\pm}(z)$, Eqs. (11) and (13) may be solved keeping these amplitudes fixed. To this end, the optical intensity is expanded to lowest order in $a_{2+}(z)$, $a_{2-}(z)$ as

$$\begin{aligned} I(\mathbf{r}) &\approx I_0(r,z) + I_1(\mathbf{r}) = I_0(r,z) + \\ &2\mathrm{Re}\left[a_{1+}^*(z) a_{2+}(z) e^{i\Delta\beta z} + a_{1-}^*(z) a_{2-}(z) e^{-i\Delta\beta z} \right] R_1(r) R_2(r) \frac{x}{r} \end{aligned} \tag{24}$$

and the local gain as

$$\frac{g_0(z)}{1 + \frac{I(\mathbf{r})}{I_{sat}(z)}} \approx \frac{g_0(z)}{1 + \frac{I_0(r,z)}{I_{sat}(z)}} \left(1 - \frac{I_1(\mathbf{r})}{I_{sat}(z) + I_0(r,z)} \right) \tag{25}$$

Under these approximations, $\Delta\varepsilon_{12}$, $\Delta\varepsilon_{22}$ may be expressed as

$$\Delta\varepsilon_{12}(z) \approx \left(G_{12}(z) - i\frac{n_0}{k_0} g_{12}(z) \right) 2\mathrm{Re}\left[a_{1+}^*(z) a_{2+}(z) e^{i\Delta\beta z} + a_{1-}^*(z) a_{2-}(z) e^{-i\Delta\beta z} \right] \tag{26}$$

$$\Delta\varepsilon_{22}(z) \approx i\frac{n_0}{k_0} g_{22}(z) + G_{22}(z) \left[\mid a_{1+}(z) \mid^2 + \mid a_{1-}(z) \mid^2 \right] \tag{27}$$

$$g_{12}(z) = g_0(z) \int_0^{r_d} dr\, r \frac{R_1^2(r) R_2^2(r)}{I_{sat}(z) + 2I_0(r,z) + \frac{I_0^2(r,z)}{I_{sat}(z)}} \tag{28}$$

$$G_{12}(z) = \frac{\eta \left(\frac{\omega_p}{\omega} - 1 \right)}{2\pi\kappa} g_0(z) \int_0^{\infty} dr\, r R_1(r) R_2(r) \int_0^{r_d} dr' r' R_1(r') R_2(r') \frac{G_1(r,r')}{\left(1 + \frac{I_0(r,z)}{I_{sat}(z)} \right)^2} \tag{29}$$

$$g_{22}(z) = g_0(z) \int_0^{r_d} dr\, r \frac{R_2^2(r)}{1 + \frac{I_0(r,z)}{I_{sat}(z)}} \tag{30}$$

$$G_{22}(z) = \frac{\eta \left(\frac{\omega_p}{\omega} - 1 \right)}{2\pi\kappa} g_0(z) \int_0^{\infty} dr\, r R_2^2(r) \int_0^{r_d} dr' r' R_1^2(r') \frac{G_0(r,r')}{\left(1 + \frac{I_0(r,z)}{I_{sat}(z)} \right)} \tag{31}$$

Inserting these expressions into Eqs. (11) and (13) and keeping only terms phase-matched in $\Delta\beta$, one obtains

$$\frac{da_{2+}}{dz} = \gamma_+(z) a_{2+}(z) + \delta(z) a_{2-}^*(z) \tag{32}$$

#262186 Received 30 Mar 2016; revised 27 May 2016; accepted 6 Jun 2016; published 9 Jun 2016

$$\frac{da_{2-}^*}{dz} = -\gamma_-(z)a_{2-}^*(z) - \delta^*(z)a_{2+}(z) \tag{33}$$

$$\gamma_+(z) = \frac{1}{2}\left\{ g_{22}(z) - \frac{ik_0}{n_0}\left[\mid a_{1+}(z) \mid^2 + \mid a_{1-}(z) \mid^2 \right] G_{22}(z) - \left[g_{12}(z) + \frac{ik_0}{n_0} G_{12}(z) \right] \mid a_{1+}(z) \mid^2 \right\} \tag{34}$$

$$\gamma_-(z) = \frac{1}{2}\left\{ g_{22}(z) - \frac{ik_0}{n_0}\left[\mid a_{1+}(z) \mid^2 + \mid a_{1-}(z) \mid^2 \right] G_{22}(z) - \left[g_{12}(z) + \frac{ik_0}{n_0} G_{12}(z) \right] \mid a_{1-}(z) \mid^2 \right\} \tag{35}$$

$$\delta(z) = -\frac{1}{2}\left[\frac{ik_0}{n_0} G_{12}(z) + g_{12}(z) \right] a_{1+}(z)a_{1-}(z) \tag{36}$$

The $\gamma_\pm$-terms in these equations describe amplifier gain and cross-phase modulation of the weak HOM modes by the strong FM modes. The G_{12} terms in $\gamma_\pm$ represent the interaction of the HOM with the thermo-optic grating inscribed by its interference with the co-propagating FM. As discussed in the introduction, this interaction does not lead to power transfer between FM and HOM when they both have the same optical frequency. Such power transfer is instead described by the δ-terms. It should be stressed that this power transfer takes place between co-propagating modes, although the mathematical structure of Eqs. (32) and (33) may suggest a scattering between opposite propagation directions. What these terms express is scattering between co-propagating modes on the thermo-optic grating set up by the interference between the modes propagating in the opposite direction. It is this effect that decisively distinguishes the double-pass amplifier from the single-pass case.

Eqs. (32) and (33) are conveniently solved by a transfer-matrix approach [12]. Introducing a discretized z-grid with spacing Δz and N gridpoints, one may write

$$a_{2+}(z+\Delta z) = t_{11}(z)a_{2+}(z) + t_{12}(z)a_{2-}^*(z) \tag{37}$$

$$a_{2-}^*(z+\Delta z) = t_{21}(z)a_{2+}(z) + t_{22}(z)a_{2-}^*(z) \tag{38}$$

$$t_{11}(z) = 1 + \gamma_+(z)\Delta z;\ \ t_{12}(z) = \delta(z)\Delta z \tag{39}$$

$$t_{21}(z) = -\delta^*(z)\Delta z;\ \ t_{22}(z) = 1 - \gamma_-(z)\Delta z \tag{40}$$

The full propagation from z=0 to z=L can then be expressed as

$$a_{2+}(L) = T_{11}a_{2+}(0) + T_{12}a_{2-}^*(0) \tag{41}$$

$$a_{2-}^*(L) = T_{21}a_{2+}(0) + T_{22}a_{2-}^*(0) \tag{42}$$

$$\overline{\overline{T}} = \prod_{i=1}^{N} \overline{\overline{t}}(z_i) \tag{43}$$

The boundary condition Eq. (17) leads to the expressions

$$a_{2-}^*(L) = a_{2+}^*(L)R_2^* \tag{44}$$

$$\Downarrow$$

$$a_{2+}(0)T_{21} + a_{2-}^*(0)T_{22} = R_2^*\left(a_{2+}^*(0)T_{11}^* + a_{2-}(0)T_{12}^* \right) \tag{45}$$

$$a_{2-}(L) = a_{2+}(L)R_2 \tag{46}$$

$$\Downarrow$$

$$a_{2+}^*(0)T_{21}^* + a_{2-}(0)T_{22}^* = R_2\left(a_{2+}(0)T_{11} + a_{2-}^*(0)T_{12} \right) \tag{47}$$

#262186 Received 30 Mar 2016; revised 27 May 2016; accepted 6 Jun 2016; published 9 Jun 2016

These equations are solved by

$$a_{2+}(L) = \frac{a_{2+}(0)\left(T_{11} - \frac{T_{12}T_{21}}{T_{22}}\right) + a_{2+}^{*}(0)R_2^{*}\left(T_{11}^{*} - \left(\frac{T_{12}T_{21}}{T_{22}}\right)^{*}\right)\frac{T_{12}}{T_{22}}}{1 - \frac{|T_{12}|^2}{|T_{22}|^2}r_2^2} \tag{48}$$

$$a_{2-}(0) = \frac{R_2 a_{2+}(L) - T_{21}^{*}a_{2+}^{*}(0)}{T_{22}^{*}} \tag{49}$$

Due to the linearization in the HOM amplitudes, the propagation equations now have a unique solution. It is noteworthy that $a_{2+}(L)$, and therefore $a_{2-}(0)$ will diverge when $|\,T_{22}\,|^2 = |\,T_{12}\,|^2 r_2^2$. Obviously, the undepleted-pump approximation will not be valid in this case. Nevertheless, the approach to this divergence is the root of the static modal instability, as shown in the next section.

3. Numerical results and discussion

Unless otherwise stated, the simulations in this paper consider a step-index double-clad fiber having a signal core with a radius of 20 μm, a V-parameter of 3, and Yb-doping with a small-signal pump absorption of 300 dB/m at 976 nm. The pump cladding radius R_p=100 μm, and the total fiber length L=1 m. Pump power is injected in the signal input/output end (forward pumping), and the signal is assumed to be fully reflected at the far end. Regarding the input seed power for the signal, 99% of it is assumed to go into the FM, and the remainder into the HOM.

For evaluating the transverse integrals in Eq. (8), (14) and (15), a radial-angular grid with 200 points in the radial direction, from r=0 to r=R_p, and 10 points in the angular direction, from 0 to 2π, was used. These parameters were found to give adequate convergence when performing the integrations by Simpson's rule [13]. Note that the transfer-matrix equations only contain radial integrals, which were evaluated on the same radial grid.

Two different numerical approaches for solving Eqs. (10)-(13) have been investigated. In a first attempt, a starting guess for $a_{1-}(0)$, $a_{2-}(0)$ was chosen, the equations were propagated forward from z=0 to z=L using a fourth-order Runge-Kutta (RK4) method [13], $a_{1-}(L)$ and $a_{2-}(L)$ were set from the resulting values of $a_{1+}(L)$, $a_{2+}(L)$ using Eq. (17), and the equations were propagated backwards from z=L to z=0. The resulting values for $a_{1-}(0)$, $a_{2-}(0)$ were used as starting points for a new pass and the procedure was iterated until a converged solution was obtained. This numerical method is efficient at low and moderate pump powers, but eventually ceases to converge. To obtain solutions over a broader range of pump powers, a Newton-Raphson, or multidimensional steepest descent, method was utilized [13]. In this method, the RK4 method is again used to forward-propagate Eqs. (10)-(13), and the differences $D_1 = a_{1-}(L) - R_1 a_{1+}(L)$ and $D_2 = a_{2-}(L) - R_2 a_{2+}(L)$ are evaluated. The goal of the method is to make both of these differences zero, which is obtained by repeated steepest-descent estimates of the desired $a_{1-}(0)$, $a_{2-}(0)$ values, until the magnitudes of the D_m are below a chosen threshold. Derivatives of the D_m with respect to real and imaginary parts of $a_{1-}(0)$, $a_{2-}(0)$ are evaluated numerically by repeated RK4 forward propagations with slightly shifted starting amplitudes. This method was found to be efficient when stepping the pump power up or down in small increments, using the solution from the previous pump power level as a starting point for steepest-descent calculations at the next level. To initiate this process, transfer-matrix solutions were obtained over a broad range of pump powers, which was straightforward, and the Newton-Raphson calculations were started at various power levels where the transfer-matrix solutions had a small HOM fraction at the output, and could therefore be expected to be reliable.

In Fig. 1 the HOM power fraction of the solutions identified by this procedure for a seed power of 1 W are plotted as a function of pump power. The solid red lines illustrate the transfer-

#262186 Received 30 Mar 2016; revised 27 May 2016; accepted 6 Jun 2016; published 9 Jun 2016

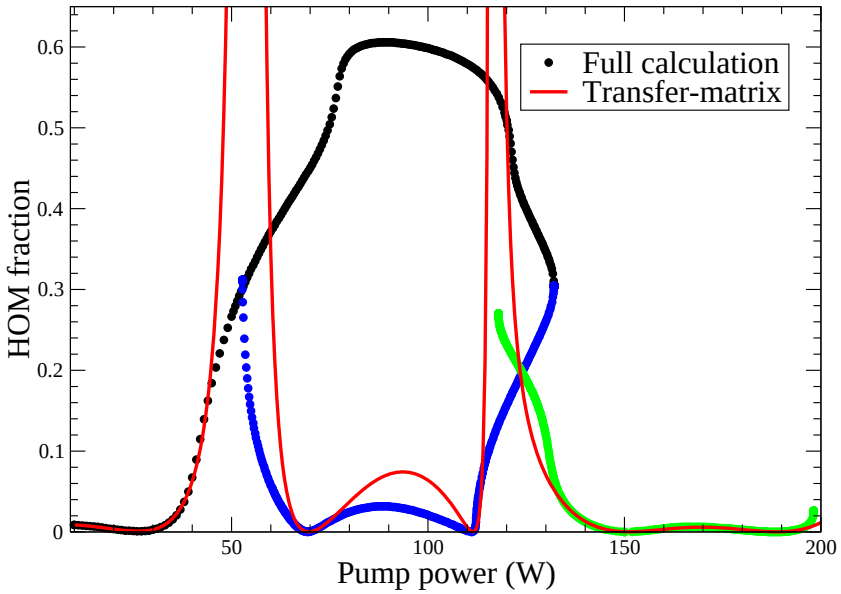

Fig. 1. Fraction of HOM output power versus pump power for the solutions of Eqs. (10-13) (filled black/blue/green circles), as well as the approximate transfer-matrix solution (solid red curve).

matrix solution, whereas black, green and blue circles indicate solutions of the full equations. The transfer-matrix solutions are seen to match the full solutions closely until a pump power level of $\sim$45 W, where the HOM fraction increases strongly. The HOM fraction of the transfer-matrix solution becomes >1 for pump powers between 50 and 60 W, an unphysical result which is possible because depletion of the FM power is neglected. The full solution is seen to level out around a HOM fraction of 0.6. Remarkably, a second solution (blue circles in Fig. 1), with a lower HOM fraction exists in a region between 53 W and 132 W pump power. Around 132 W it merges with the high-HOM solution, whereas the two solutions are distinct around 53 W, even if they also here converge to roughly the same HOM fraction. It was not possible to track the second (lower) solution below 52.8 W pump power. More research is needed to clarify if the solution actually vanishes at this point, or if it reflects a shortcoming of the numerical method used. A third solution (green circles in Fig. 1) was found by starting the Newton-Raphson algorithm on a transfer-matrix solution at a pump power of 150 W, and tracking it towards lower as well as higher powers. This solution could not be tracked below a pump power of 118 W. The vanishing of these numerical solutions occurs close to, but not exactly on top of, the divergencies in the transfer-matrix solution.

The system is at least bistable between pump powers of 53 and 118 W, and tristable between 118 W and 132 W. At pump powers <45 W and >135 W the transfer-matrix solution closely approximates the single full solution obtained. On the other hand, at intermediate pump powers there are significant deviations between the transfer-matrix solution and the low-HOM solution of the full equations, even at HOM fractions below 1%, indicating that the equations are highly

#262186 Received 30 Mar 2016; revised 27 May 2016; accepted 6 Jun 2016; published 9 Jun 2016

sensitive to approximations in this region. Just before 200 W there is an upturn in the full solution, and it was in fact not possible to track it further, indicating that a new instability region may be coming up. In general it must be remarked that the current calculations may prove the existence of instabilities, by finding solutions with high HOM fractions. The correctness and convergence of these solutions could be carefully checked. It is, however, harder to prove the existence of stable regions with low HOM fractions, because one must then prove that all solutions of Eqs. (10)-(13) have been found for a given pump power level.

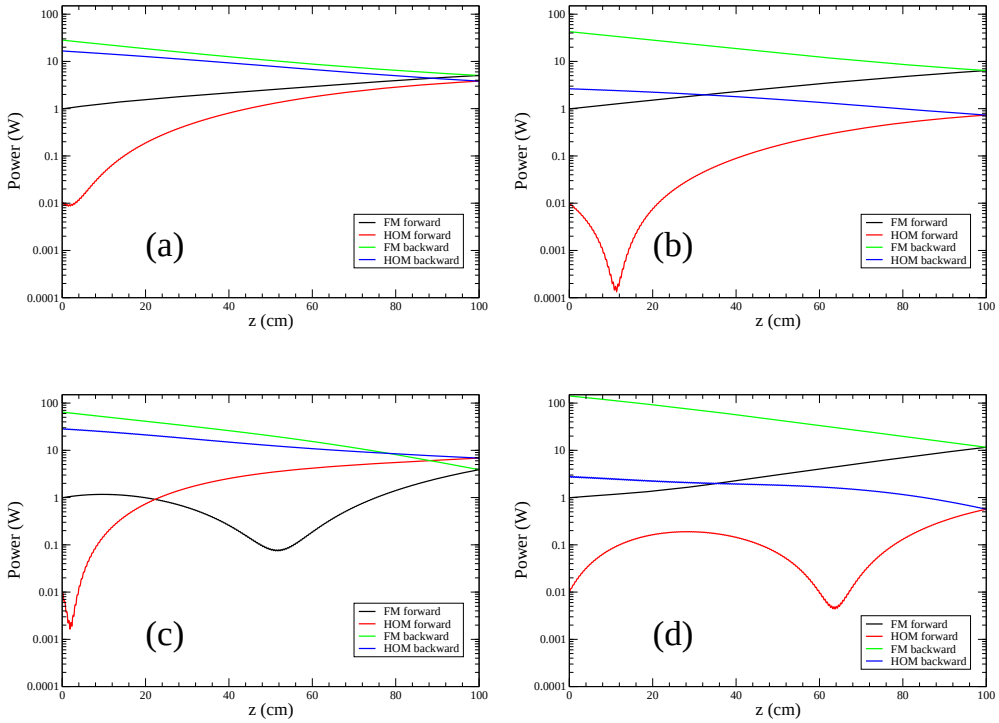

Fig. 2. Modal power distribution along z for forward- and backward-propagating fields in four selected cases: (a) 60 W pump, high HOM fraction, (b) 60 W pump, low HOM fraction, (c) 132 W pump high HOM fraction, (d) 198 W pump.

In Fig. 2, the signal power in forward- and backward-propagating FM and HOM modes is plotted as a function of z for four different solutions: The two solutions with high and low HOM content found at a pump power of 60 W; the solution with high HOM content found for a pump power of 132.06 W where the two upper solution branches merge in Fig. 1; and the solution found at a pump power of 198 W. The most interesting structure is found in the evolution of the forward-propagating modal powers, especially those of the HOM. This may be understood as follows: Since it has been proved that the thermal grating formed by two copropagating modes cannot transfer power between these modes in the static limit [2, 3], power transfer between a pair of such modes must be due to the grating set up by the light propagating in the opposite direction. The strongest grating section in the fiber is the one set up by the backward-propagating modes close to the signal input/output end, because this is where signal power is strongest. Thus, it is the forward-propagating modes at the input end which are most susceptible to scattering and power exchange between FM and HOM.

#262186 Received 30 Mar 2016; revised 27 May 2016; accepted 6 Jun 2016; published 9 Jun 2016

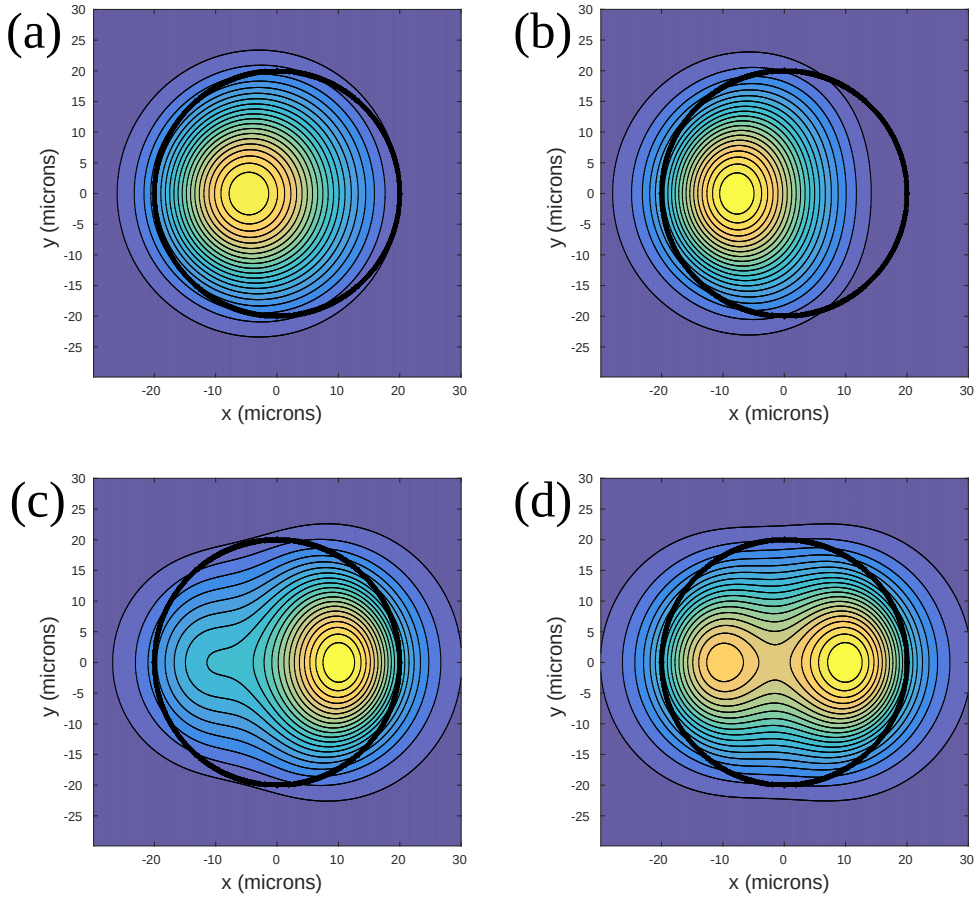

Fig. 3. Spatial output power distribution for a selection of the solutions with high HOM fraction shown in Fig. 1: (a) 40 W pump, (b) 50 W pump, (c) 85 W pump, (d) 90 W pump. The black circle indicates the core boundary. Contour levels are on a linear scale.

#262186 Received 30 Mar 2016; revised 27 May 2016; accepted 6 Jun 2016; published 9 Jun 2016

These plots give an interesting physical insight into the nature of the multistability. Comparing the two solutions at 60 W pump power, one sees that the one with a high HOM fraction at the output also shows a rapid growth of the forward-propagating HOM to a level of ∼1 W in the first 0.5 m of the amplifier. In the low-HOM solution, this power level is not reached by the forward-propagating HOM even at the end of the amplifier. The strong initial scattering leads to a high backward propagating HOM fraction, and thus a strong grating from the backward propagating modes. This grating is what scatters the forward-propagating modes, making the high-HOM solution self-consistent. Conversely, a weak initial scattering leads to a weak grating from backward propagating modes, which makes the low-HOM solution self-consistent. This qualitatively explains why several different solutions may stabilize for given initial values of pump and signal powers.

It is important to note that grating strength is not the only important parameter. The direction of power flow in a long-period grating depends on the relative phases of the fields and the grating. In the high-HOM solution, efficient power transfer to the forward-propagating HOM is seen to appear almost from the launch end, whereas in the low-HOM solution the initial power transfer goes from the HOM towards the FM. Thus the field phases are also of crucial importance in determining the structure of the solutions. The relative phases of fields and gratings evolve through the fiber due to the thermal nonlinearity, and this evolution becomes more complex as the power increases. At the highest pump power of 198 W, the direction of power transfer in the forward-propagating fields is seen to reverse two times.

To illustrate the importance of these results for the spatial shape of the amplifier output, some examples of output field profiles are plotted in Fig. 3. All fields are for the solution with highest HOM content at the specified pump power. Already at a pump power of 40 W, the few percent of HOM admixture leads to a noticeable shift of the mode profile away from the core center. At 50 W pump power the field profile is still approximately circular, but shifted almost half the core radius from the center. At 85 and 90 W, the profiles become more complex, and are seen to evolve with pump power even though the HOM fraction varies little in this region. This is due to the evolution of the relative phase between the modes at output.

The calculations presented so far predict a very low threshold for onset of modal deformations of ∼40 W pump power or ∼30 W FM signal power. Obviously, this threshold will depend on the fiber and system design. While a full exploration of the design parameter space is outside the scope of the present work, Fig. 4 shows two examples of how the deformation threshold may be improved by changing the fiber design. The figure shows the initial approach to the instability, *i.e.* a calculation started at low pump powers and stepped up in power using the Newton-Raphson algorithm described above. In one case, the core Yb concentration and the pump cladding area have both been doubled, to lower the inversion level in the core, thereby suppressing the thermo-optic nonlinearity by gain saturation [11, 14, 15]. In another case, the V-parameter of the core was reduced to 2.5, thereby reducing the confinement of the HOM and its coupling to the FM [3]. The results are compared to the low-power branch of the solution found for the 'reference' fiber described above. It can be seen that both approaches are effective in raising the threshold for strong HOM coupling, which for the V=2.5 fiber increases to around 88 W pump power, or 65 W total signal power (FM and HOM).

Finally, it is of interest to study the influence of amplifier system parameters on the onset of modal deformations. In Fig. 5, the impacts of three different system-related modifications are compared with the 'reference' calculation. The modifications are reduction of signal seed power to 100 mW, reduction of HOM seed level to 1 ‰, or 10 mW for a signal seed level of 1 W, and finally a change of ϕ_2 to 1, *i.e.* a π-phaseshift of the HOM relative to the FM in reflection. None of these modifications are seen to have a major impact on the threshold for modal deformations. It is particularly interesting to notice that an order-of-magnitude reduction

#262186 Received 30 Mar 2016; revised 27 May 2016; accepted 6 Jun 2016; published 9 Jun 2016

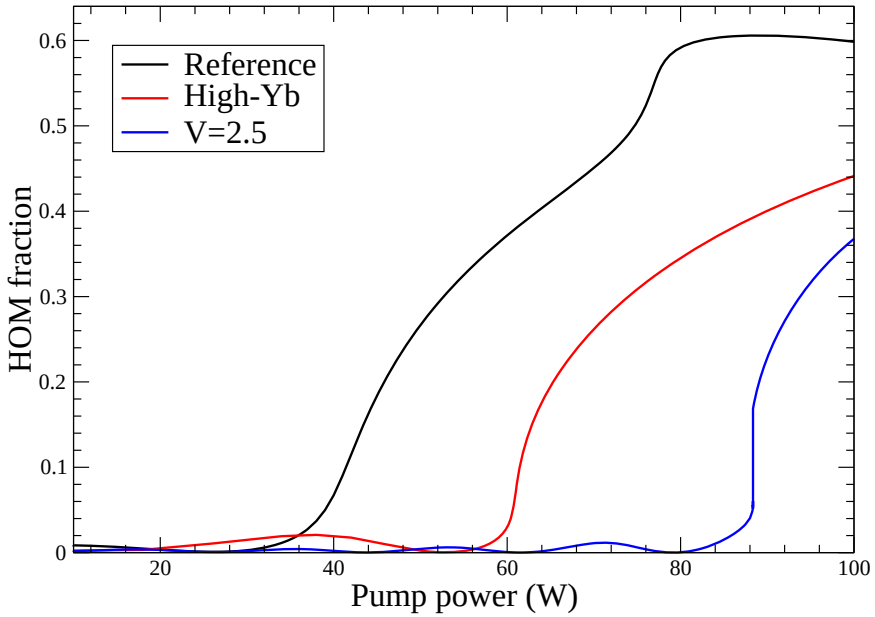

Fig. 4. Fraction of HOM output power versus pump power for the 'reference' fiber, as well as for a fiber with doubled Yb concentration and pump cladding area ('High Yb') and one with a V-parameter of 2.5.

in the HOM seed fraction only leads to a marginal upwards shift of the deformation threshold. The slight sensitivity of the HOM fraction to the relative phase shift in reflection may imply that thermal drifts in the system may lead to a drift in the output beam profile, depending on how the reflection is realized. The same thing may of course be expected from thermal drifts in the relative phase of FM and HOM on input.

4. Comparison to experimental results

The theory put forward in the present paper predicts a static thermo-optic mode deformation with regions of multistability appearing in double-pass fiber amplifiers at lower power thresholds than the well-known dynamic modulational instability. To the best of the authors knowledge, no clear experimental description of such a phenomenon has as yet been published. Jauregui *et al* mentioned experiments finding a factor-of-two reduction of the modal instability threshold in bidirectional fiber amplifiers, but did not provide details on the nature of the instability [16]. In a very recent publication [17], Antipov *et al* showed experimental evidence of a strongly reduced dynamic modal instability threshold in a single-pass amplifier caused by back-reflections from the amplifier end facet. These authors also presented a detailed model, having many similarities with the present work, although focusing on dynamical instabilities and low back-reflection coefficients. On the other hand, Hejaz *et al* demonstrated a high power CW laser cavity showing an instability threshold of $\sim$500 W pump power (337 W signal power), which could be shifted beyond 800 W pump power (500 W signal power) by reducing

#262186 Received 30 Mar 2016; revised 27 May 2016; accepted 6 Jun 2016; published 9 Jun 2016

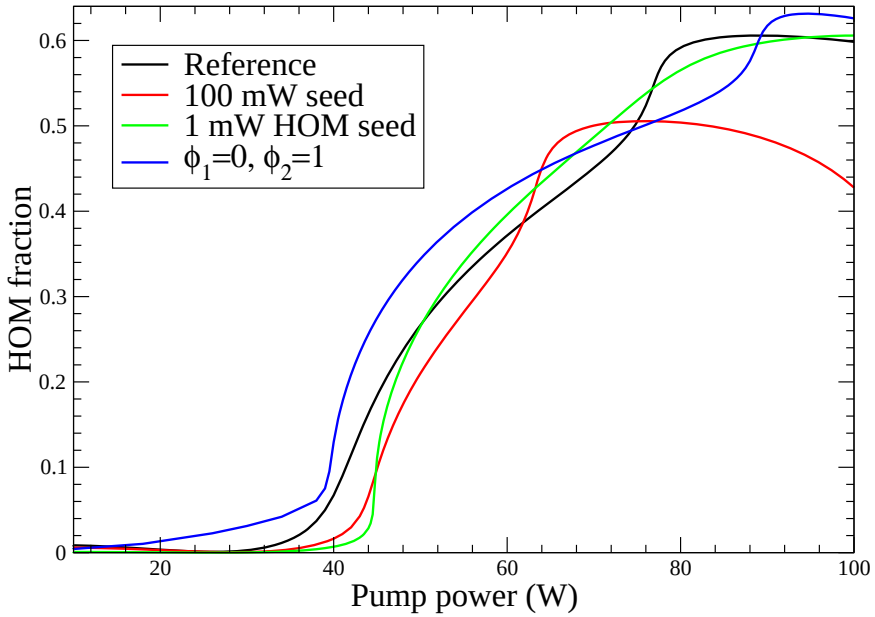

Fig. 5. Fraction of HOM output power versus pump power for the 'reference' configuration, as well as for systems with 100 mW seed power, 1 mW HOM seed (corresponding to 0.1% of the total seed), or a π phase shift between FM and HOM in the reflection.

the pump wavelength and coiling the fiber for HOM suppression [18]. The instability threshold was determined from the slope efficiency curve, and so its nature (static/dynamic) is not entirely clear from the results presented. While a laser cavity has many similarities with a double-pass amplifier, there are also differences, especially in the CW case as noted in Section 2. Therefore the current theory cannot be directly applied to this interesting case. In addition, the use of narrow-band fiber gratings by Hejaz *et al* to form the cavity could lead to significant HOM suppression. Also, the cavity length of 18.5 m may have served to increase the instability threshold compared to the simulations presented here, because it moves the oscillator into a highly saturated regime, which increases the threshold as evidenced by the results shown in Fig. 4 for the high-Yb fiber design.

In summary, while existing literature does not presently provide clear experimental support for the theory presented, neither does it appear to contain clear falsifications. Detailed experimental studies of high-power double-pass amplifiers would therefore be of immediate interest.

5. Conclusion

In conclusion, an existing formalism for describing dynamical mode instabilities in single-pass fiber amplifiers has been extended to the case of a double-pass amplifier in the static limit. It is shown that a static deformation of the output signal field may be induced by thermo-optic nonlinear effects at a power threshold much lower than those commonly found for dynamical

#262186 Received 30 Mar 2016; revised 27 May 2016; accepted 6 Jun 2016; published 9 Jun 2016

instabilities in single-pass amplifiers. The coupled-mode equations describing the phenomenon display a rich structure, with regions of multistability, and rapid transitions in the power distribution between fundamental and higher-order modes. Clearly, more research is needed to clarify the dependence of the modal deformations on fiber and system design, as well as its influence on dynamical instability effects in double-pass amplifiers.

Acknowledgments

Fruitful discussions with Kristian Lundgaard Jensen and Thomas Tanggaard Alkeskjold are gratefully acknowledged. The author acknowledges financial support from the Danish Council for Independent Research - Technology and Production Sciences (FTP).

#262186 Received 30 Mar 2016; revised 27 May 2016; accepted 6 Jun 2016; published 9 Jun 2016